Nuclear Engineering and Technology 53 (2021) 2357–2363

Contents lists available at ScienceDirect

Nuclear Engineering and Technology

journal homepage: www.elsevier.com/locate/net

Original Article

Effects of electronic energy deposition on pre-existing defects in 6H–SiC

Wenlong Liao, Huan He, Yang Li, Wenbo Liu, Hang Zang, Jianan Wei, Chaohui He*

School of Nuclear Science and Technology, Xi'an Jiaotong University, Xi'an, 710049, China

ARTICLE INFO

Article history:
Received 9 July 2020
Received in revised form
17 January 2021
Accepted 19 January 2021
Available online 22 January 2021

Keywords:
2T-MD model
Defect recovery
Electronic energy loss
6H–SiC

ABSTRACT

Silicon carbide is widely used in radiation environments due to its excellent properties. However, when exposed to the strong radiation environment constantly, plenty of defects are generated, thus causing the material performance downgrades or failures. In this paper, the two-temperature model (2T-MD) is used to explore the defect recovery process by applying the electronic energy loss (Se) on the pre-damaged system. The effects of defect concentration and the applied electronic energy loss on the defect recovery process are investigated, respectively. The results demonstrate that almost no defect recovery takes place until the defect density in the damage region or the local defect density is large enough, and the probability of defect recovery increases with the defect concentration. Additionally, the results indicate that the defect recovery induced by swift heavy ions is mainly connected with the homogeneous recombination of the carbon defects, while the probability of heterogeneous recombination is mainly dependent on the silicon defects.

1. Introduction

Silicon carbide (SiC) possesses quite a few excellent physical and chemical properties, such as high thermal conductivity, high chemical stability, good radiation resistance, wide energy gap [1]. Based on these superiorities, SiC is widely recognized as a kind of potential material that can work in radiation conditions. SiC possesses various polytypes, as we all know, hexagonal (2H-, 4H-, and 6H–SiC) and cubic (3C–SiC) configurations [2]. Since these polytypes own different properties, hexagonal configurations SiC are semiconductor materials used in electronic devices; cubic SiC is a kind of ceramic material used as the structural components in fusion reactors [3], cladding material for gas-cooled fission reactors and inert matrix for the transmutation of plutonium and other transuranic [4] on account of its small capture cross-sections for cosmic rays and neutrons. Electronic devices fabricated from hexagonal SiC can work reliably and efficiently at elevated temperatures and in highly radioactive environments [5].

On the heels of the high energy ion irradiation, interaction between incident ions and target materials will take place, leading to energy transfers from the projectile to both target nuclei and electrons. The incident ions with high kinetic energy are slowed down by exciting electrons along the ion track, reversely, elastic collision with atoms turns into the dominant retardation mechanism at lower ion energy (keV) [6]. Generally, these two processes are quantified by the electronic and nuclear stopping respectively, representing the loss of energy per unit length of the ion trajectory. The nuclear energy loss (Sn) leads to atomic displacements and collision cascades, producing defects and defect clusters. Relatively, the electronic energy loss (Se) results in the excitation of the electronic system, and subsequently part of this energy return to the atomic system via the electron-phonon (e-p) interactions [7].

Over the past 20 years, there have been a large number of simulations on displacement damage with classical molecular dynamics (MD) simulations. And a large number of vital information on the defect production and early radiation processes due to Sn have been obtained [8–12].However, the simulation about ionization effects hasn't been adequately understood until now [13]. It is because the inelastic interactions, non-equilibrium processes, and material-dependent behavior must be taken into account with the participation of the ionization effects on the process of radiation. But there are increasing experiments carried out about the defect annealing and damage recovery of SiC due to the Se these years [14–20]. With respect to the damage recovery, Zhang Y et al. [21] performed two-step irradiation in perfect SiC crystalline where defects were first created in the material by low energy particles

* Corresponding author.
E-mail address: hechaohui@mail.xjtu.edu.cn (C. He).

https://doi.org/10.1016/j.net.2021.01.017

and subsequently irradiated with swift heavy ions (SHI) with energy larger than several hundred MeV (Se $>20\text{keV}\cdot\ nm^{-1}$) [22–24]. And they argued that the energy transferred to the electron system of SiC by energetic ions via inelastic ionization can effectively anneal pre-existing defects and restore the structural order. Besides, no ion tracks have been captured in the semiconductor SiC, and SHI irradiation has been found to yield either no structural damage [25] or only point defects [26]. What's more, Zhang Y et al. [21] also draw attention to ionization effects at a lower energy regime (Se $\approx 5 \sim 10\text{keV}\cdot nm^{-1}$), where both Sn and Se should be taken into consideration. M.Backman et al. [6] simulated the effect of 870 MeV Pb (Se $= 33\text{keV}\cdot nm^{-1}$) impacts on different models with uniform concentration structural defects in 3C–SiC at room temperature, and they found the significant recovery of point defects as well as recrystallization at the amorphous-to-crystalline interface of an amorphous layer. But the relationship between the recovery of defects induced by single primary knock-on atoms (PKA) and the Se is still unknown, which is indispensable for understanding the mechanism of defect recovery induced by different Se.

2. Methods

In this simulation, two-step irradiation was performed on 6H–SiC, in which a single PKA (with kinetic energy 2 keV, 3 keV, 4 keV, and 5 keV) was firstly injected and subsequently irradiated with high energy ions at room temperature. All the radiation processes were simulated by DL_POLY [27].

Equilibration of the systems under the constant pressure and temperature (NPT) ensemble with a constant time step preceded in the irradiation. For the classical MD simulation, the constant volume and energy (NVE) ensemble was used. The cascade simulations employ a variable time step to describe the irradiation dynamics. Atom Si was chosen as the primary knock-on atom (PKA) for its mass is higher than C, which would transfer more energy when the collision happened. And Si was injected from the center of the top layer, along with the [4 11–95] direction (just off Z-direction) for minimizing the possibility of the tunneling effect in the cascade formation. As shown in Fig. 1, to avoid the translation of the system after the implantation of PKA, the mass center of the whole system must be kept constant and the linear momentum of each atom should be zero at each step of the simulation [28]. Subsequently, SHI passed through the center of the system in the z-direction (five events for each case), and the cylinder represents the thermal spike deposited along with the ion track due to Se. A layer of the MD box boundaries with 5 Å width is attached to a modified Langevin thermostat [29], so that the velocities of atoms within this layer are scaled to the target temperature equal to 300 K, imitating the energy dissipation. The interaction between the atoms is modeled using the hybrid Tersoff/ZBL potential [30], since it has been widely and successfully used to model the MD simulation of SiC. The simulation size is $12.4\times\ 12.8\times\ 12.1\ \text{nm}^3$, containing roughly 180000 atoms.

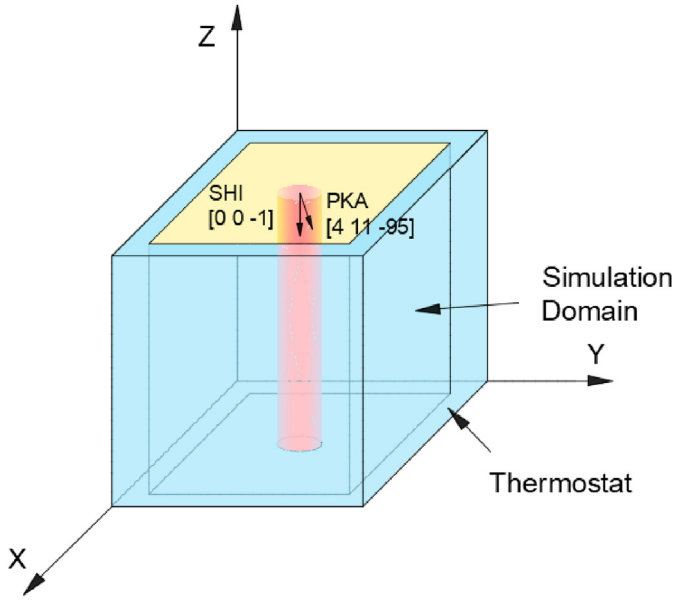

Fig. 1. The cylindrical in the center represents the electronic energy deposition after ion pass through the system in the Z direction. The thermostat is applied around the system except for Z boundary.

Wigner-Seitz method [11] is used to identify the defects, based on a complete defect-free lattice as the reference center and taking the space formed by the vertical bisectors of adjacent atom lines as the reference space, and then compare the position of the atom output by each step of the cascade collision process with the original space position. When sites are occupied by zero atoms, these sites are marked as "Vacancies". Besides, the sites occupied by more than one atom were labeled as "Interstitials". And those sites containing one atom but different from the original one are called "Anti-sites".

The SHI irradiation process is simulated by using the two-temperature (2T-MD) model [29,32] within the MD methods. As Fig. 2 (a) shows, the 2T-MD model splits the system into two coupled subsystems, the lattice subsystem and the electron subsystem, between which energy is transferred by electron-phonon coupling depending on the temperature difference. In the 2T-MD model, the SHI is slowed down by inelastic collisions with electrons, and the energy deposited into the electronic system is qualified by Se. Fig. 2 (b) gives a schematic of this simulation setup, the lattice system is split into discrete coarse-grained lattice ionic temperature (CIT) voxels, and discretizing the electronic system into coarse-grained electronic temperature (CET) voxels. Energy can thus be exchanged between the voxels and subsequently passed to or from the atoms within each respective CIT. The volume of each CIT voxel must contain a sufficient number of atoms so that thermal fluctuations of ions are negligible and an ionic temperature can be defined: a good general choice is a cube of length 10 Å in each direction [31]. There is more flexibility in choosing the number of CET voxels, as long as an integer number of these overlap with the CIT grid: this simulation divides the MD cell into $12\times 12\times 12$ (each $\approx 10\ \text{Å}^3$), a $24\times 24\times 12$ electronic temperature voxel grid extends over the MD cell in the X and Y direction. The system was pre-equilibrated for 200ps (with 1 fs timestep) using an NPT ensemble (300 K), and the SHI irradiation was simulated for 20 ps (with 1fs timestep).

In the 2T-MD model, the electronic subsystem is connected to the ions via a modified Langevin thermostat, and the equation (Eq. (1)) of motion used to describe the trajectories of the ions include an extended term based on Newton's law of motion [29,33]: the friction term and the stochastic force.

$$m_i \partial v_i / \partial t = F_i(t) - \gamma_i v_i + \tilde{F}(t) \tag{1}$$

Where m_i and v_i represent the mass and the velocity of atom i, respectively. $F_i(t)$ is the force acting on atom i due to the interaction among the surrounding atoms at time t. The energy loss to the electron is included via a friction term with damping coefficient γ_i. $\tilde{F}(t)$ (Eq. (2)) is the stochastic force, representing the energy from the electronic subsystem to the atoms by electron-phonon

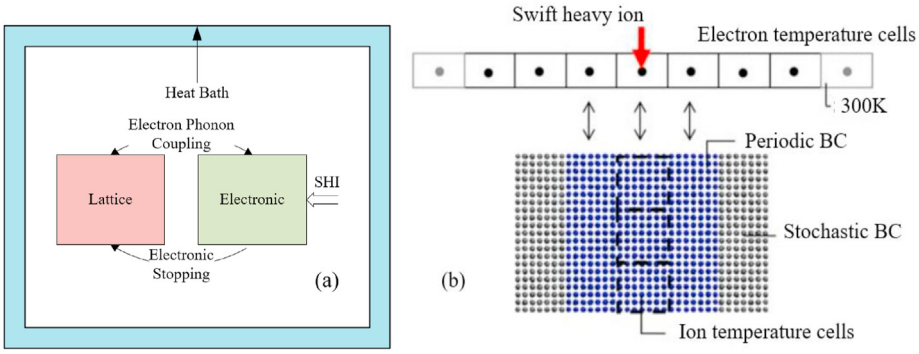

Fig. 2. (a) Schematic of thermodynamic coupling and processes in 2T-MD, (b) simulation setup for swift heavy ion impact [31].

coupling. And the magnitude of the force is related to local electronic temperature (T_e) by the fluctuation-dissipation theorem,

$$\langle \tilde{F}(t').\tilde{F}(t)\rangle = 2k_B T_e \gamma_i \delta(t'-t) \tag{2}$$

and it has a mean value of zero. The evolution of the electronic temperature (T_e) is calculated by the heat diffusion equation, (Eq. (3))

$$C_e \rho_e \partial T_e \Big/ \partial t = \nabla(k_e \nabla T_e) - g_p(T_e - T_\alpha) + A(r,t) \tag{3}$$

Where C_e is the heat capacity $C_e = 1 Jcm^{-3}K^{-1}$ [34], k_e the electronic thermal conductivity $k_e = C_e D_e$ with $D_e = 2cm^2 s^{-1}$ [34], T_e and T_α are the electronic and atomic temperatures, respectively. And electron-phonon coupling constant g_p is expressed as:

$$g_p = \frac{3Nk_B\gamma_p}{\Delta V m_i} = \frac{C_e D_e}{\lambda^2} \tag{4}$$

Where the electron-phonon mean free path λ is 5.2 nm [35], corresponding to the bandgap of 6H−SiC (3.03eV). The timescale for energy loss due to e-p interactions is:

$$\tau_p = \frac{m_i}{\gamma_p} \tag{5}$$

or from Eq. (4)

$$\tau_p = \frac{3nk_B}{g_p} \tag{6}$$

Where n is the number of atoms per volume, τ_p is 0.402ps from Eq. (6).

The A(r, t) is a source term corresponding to the energy deposited by SHI, via a spatial Gaussian and temporal exponential distribution with the mean absorption radius of 0.2735 nm using Bohr's principle of adiabatic variance [36] and a characteristic deposition time of 1 fs. [37,38].

3. Results and discussion

As mentioned above, there are two steps during the whole simulation process, displacement cascade and ionization effects by SHI. In the first step, PKA Si was injected into the system, after 12ps, the point defects became stable and were counted for the reference values in the later process. In the second step, SHI passed through the center of the system in the z-direction, and the energy deposited from SHI is quantified by the electronic stopping power (Se) which can be calculated by SRIM. In this paper, to learn the effect of SHI on the defects produced in the first step more effectively, Se is taken from 10 keV/nm to 30 keV/nm. Fig. 3 (a) shows the average surviving point defects in four simulation events before [39] and after SHI injected with different electronic energy loss. In Fig. 3 (a) the different color represents different energy PKA injected into the system in the first step, while the dashed line and the points represent the total point defects before and after SHI injected respectively, the error bar represents the standard error over five events for each case. As this figure shows, the overall trends are a little different between the four cases. When Se is lower than a certain value (near 25keV·nm^{-1}), the number of surviving point defects has almost no change in the case of low PKA energy, while the surviving defects are lower than the reference value (decrease firstly and then increase) in the case of higher PKA energy. From the spatial distribution of defects, we found that the defect density in the center area of cascade raises with PKA energy. Therefore, in this manuscript, the defect concentration refers not only to the defect density in the damage region but also the local defect density. And the defects recovery can only take place when the defects in the damage region or the local area reach a certain concentration. When Se is larger than 25keV·nm^{-1}, the point defects will increase in all cases due to the generation of C defects (V_C and I_C) in this energy range as shown in Fig. 3 (b). From Fig. 3 (b), the point defects, mainly related to V_C and I_C, will be produced after SHI injected with electronic energy loss larger than 25keV·nm^{-1} in the perfect lattice. However, the defects related to Si (containing C_{Si}, Si_C, V_{Si}, I_{Si}) are hardly induced. It is because that the formation energy of C defects is smaller than Si defects in 6H−SiC [40]. During the irradiation of SHI, the deposited energy by the inelastic collision process will raise the temperature around the ion track, intensifying the thermal vibration of the particle. When the deposited energy is large enough to break the covalent bond, the defects can be produced. Due to the smaller formation energy, the C defects dominate the generated defects. The two prime issues can be summarized: (1) the defects recovery can only take place when the defects in the damage region or the local area reach a certain concentration. (2) New point defects will be produced when Se is larger than 25keV·nm^{-1}, and the majority of new defects are C defects.

Generally speaking, the reactions among different point defects after SHI injection contain recombination and knock-out process. The knock-out process takes place between the interstitial atom and anti-site atom which will result in the defect recovery, and one moveable interstitial atom will be produced at the same time. The recombination processes, which contain homogeneous recombination and heterogeneous recombination [41,42], lead to defect recovery and the production of anti-site, respectively. In Fig. 4, the

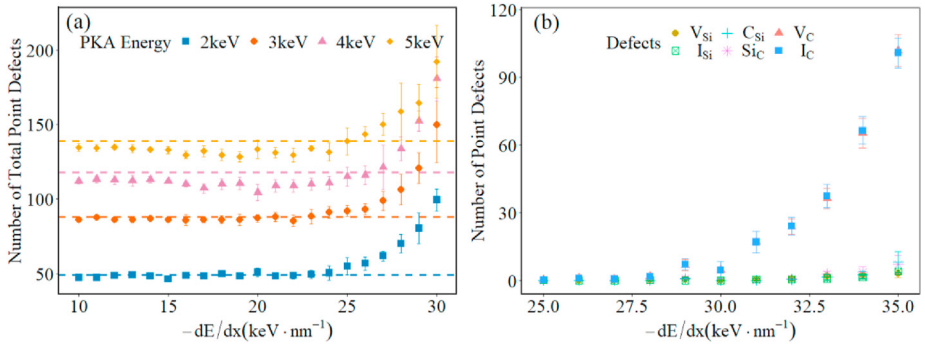

Fig. 3. (a) Average surviving number of total point defects before and after applying different electronic energy loss for the four different irradiation cases, the error bar represents the standard error over five events for each case. (b) The number of different point defects after SHI injected with different electronic energy loss in the perfect lattice.

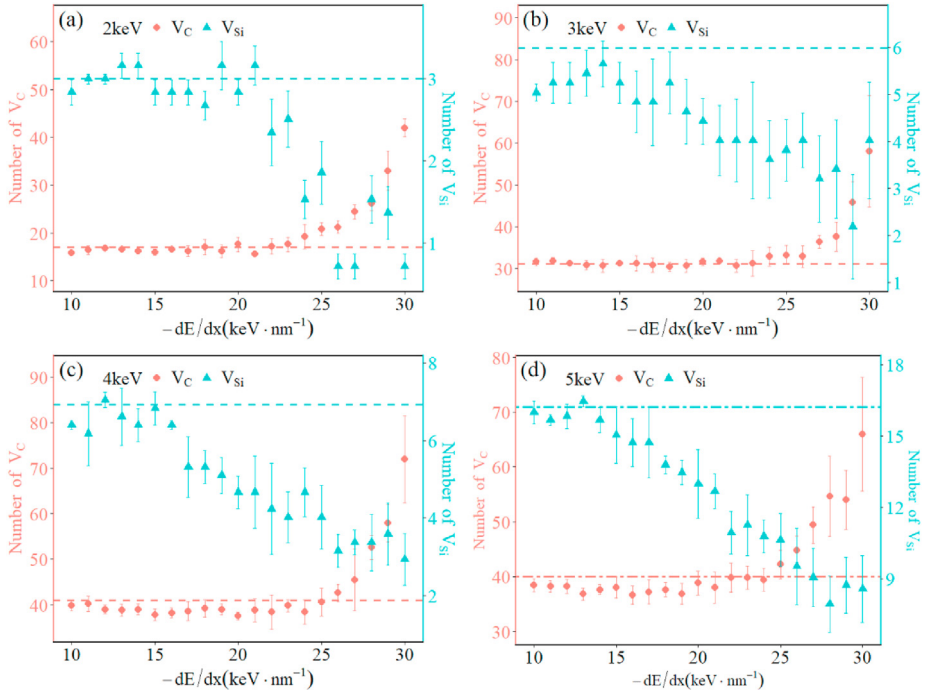

Fig. 4. The number of vacancies as a function of Se, the dashed line and points represent the number of vacancies before and after applying Se, respectively. (a)–(d) represent the different PKA energies in the first step.

vacancies were counted under four different PKA energies. For carbon vacancies (V_C), it follows the same trend as the total point defects in Fig. 3 (a), which means that the C defects dominate in the evolution of point defects. In (c) and (d), the number of V_C decreases firstly. In Fig. 3 (a), the number of total point defects decreases at this time as well, which means the homogeneous recombination happens. Then, with the growth of energy, the production of V_C gradually gained the upper hand, so V_C increased in the latter half. As for silicon vacancies (V_{Si}), the number of V_{Si} decreased gradually with the increasing Se, lower than the reference value all the time. The decrease of V_{Si} is also attributed to the two kinds of recombination, and it will be explained in detail below. Besides, the process $V_{Si} \rightarrow V_C + C_{Si}$ can also take place in 6H–SiC [43], which will reduce V_{Si} as well.

Fig. 5 shows the evolution of interstitials in different cases. For the silicon interstitials (I_{Si}), there is no obvious trend due to the low I_{Si} concentration in the system, but the surviving I_{Si} is lower than the reference I_{Si} almost over the whole Se range in each case. For the carbon interstitials (I_C), when Se is lower than 25keV· nm^{-1}, its quantity fluctuates around the reference value in the case of low PKA energy as shown in Fig. 5. (a), and its number decreases gradually with the increase of Se in the case of higher PKA energy as shown in Fig. 5. (d). Therefore, the defects recovery can only take place when the defects reach a certain concentration. By comparing Fig. 5(c) and Fig. 5(d), the I_C starts decreasing in Fig. 5 (c) for Se larger than 17 keV/nm, and it decreases more profoundly in Fig. 5 (d). From this phenomenon, it can be obtained that the defect recovery is easier to occur when the defect concentration is higher, and there is more defect recovery take place. When Se is larger than 25keV·nm^{-1}, the number of I_C increases with Se due to the new I_C defect produced by Se.

Fig. 6 shows the evolution of anti-sites in different cases. It can be seen that the overall trend of both C_{Si} and Si_C increases with Se, particularly in Fig. 6 (b) and (d). By comparing the evolution of C_{Si} with V_{Si}, it can be discovered that the decrease of V_{Si} is almost equal to the increment of C_{Si} when Se is lower than 25keV·nm^{-1}. A similar result can be found by comparing the Si_C with I_{Si}. This phenomenon reveals that the probability of heterogeneous

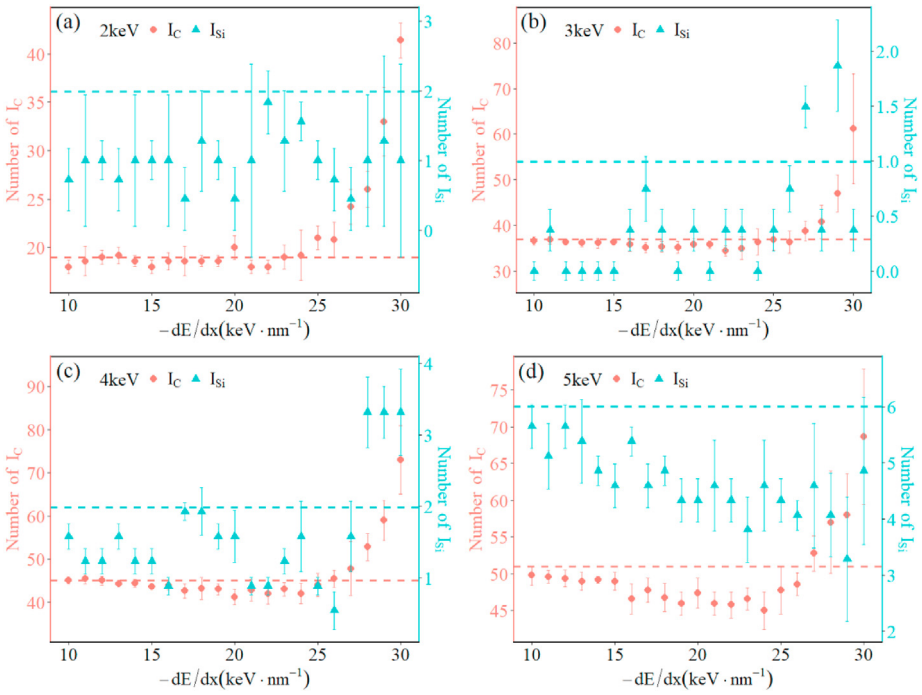

Fig. 5. The number of interstitials as a function of Se, the dashed line and points represent the number of interstitials before and after applying Se, respectively. (a)–(d) represent the different PKA energies in the first step.

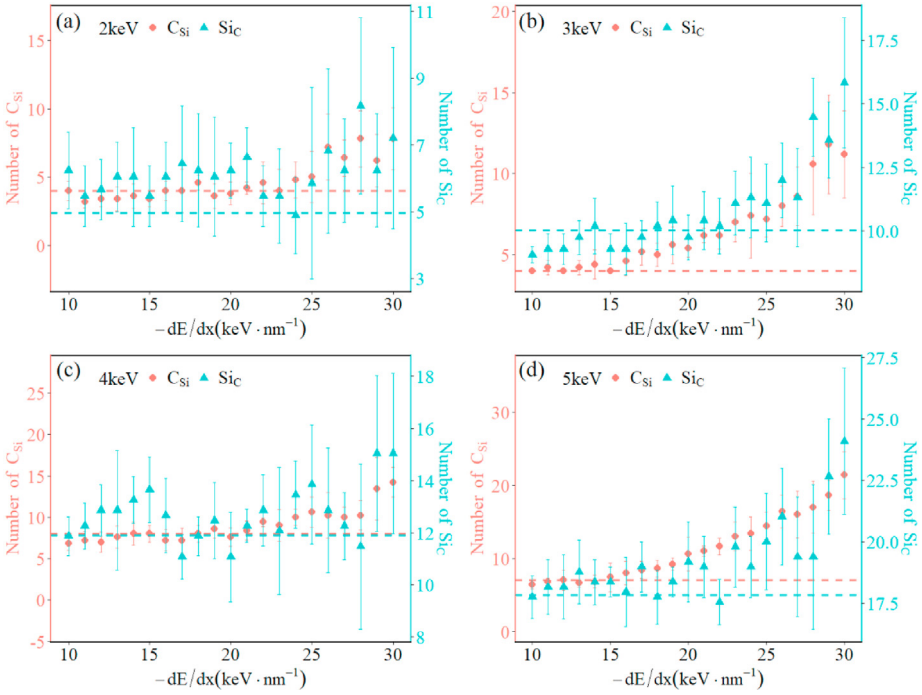

Fig. 6. The number of anti-sites as a function of Se, the dashed line and points represent the number of anti-sites before and after applying Se, respectively. (a)–(d) represent the different PKA energies in the first step.

recombination depends mainly on silicon defects. On the contrary, by comparing the surviving total number of point defects with the carbon defects, the result leads to the decrease of the total number of point defects closely connected with the decrease in the carbon defects. And this result reveals that the probabilities of homogeneous recombination mainly depends on the carbon defects [44]. Consequently, the defect recovery induced by SHI is mainly connected with the homogeneous recombination of the carbon defects.

Fig. 7 presents the temporal evolution of the lattice temperature with time for different Se, the different curves show the lattice temperature along the y dimension of the MD box. And the effects of different Se on the pre-defects can be reflected by the lattice

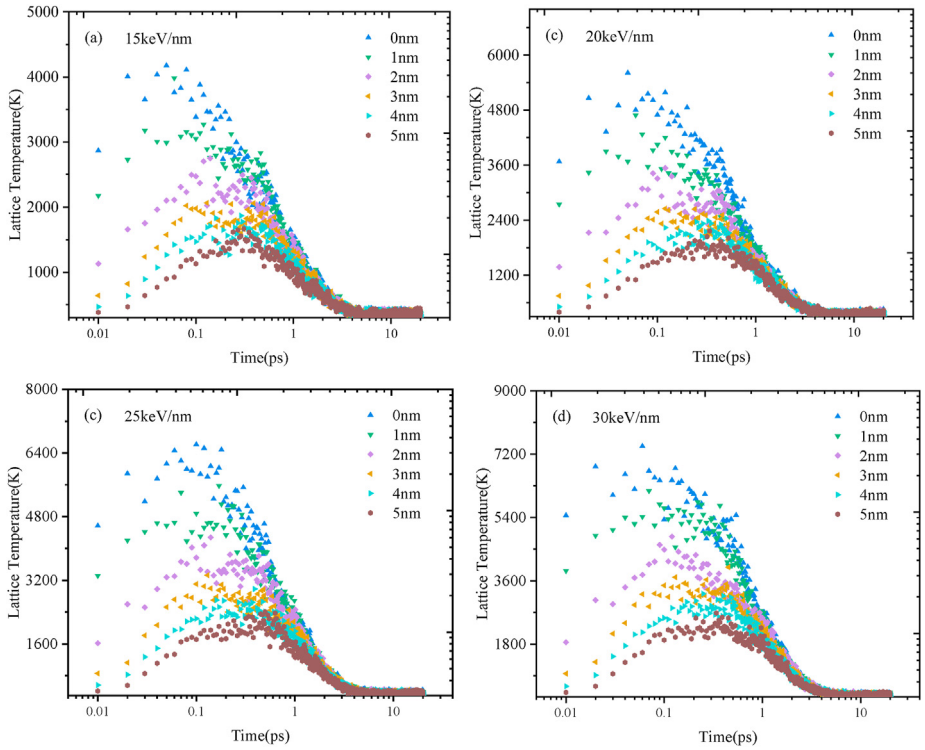

Fig. 7. Evolution of the lattice temperature with time for (a)15 keV/nm (b) 20 keV/nm (c)25 keV/nm (d)30 keV/nm Se. The different curves show the lattice temperature along the y dimension of the MD box.

temperature. As seen here, it can take up to 4 ps for the lattice system to completely cool down to the target temperature (300 K). From Fig. 7, the peaks of lattice temperature and the time to reach peak are different at different radii from the center in a simulation, but the curve's shape is the same under different Se.

4. Conclusion

In order to learn the effect of Se on the defects induced by single primary knock-on atoms (PKA), the 2T-MD model was used to obtain the evolution of point defects after the injection of SHI. In the simulation, four PKA energies were taken to explore the influence of defect concentration on the defect recovery. The results indicate that almost no defect recovery takes place until the defect concentration is large enough, and the recovery of defects becomes more remarkable with the increasing defect concentration. Besides, the number of total defects is calculated under different Se, and the results indicate that the local heating due to the high electronic stopping of SHI can lead to the recovery of defects when Se is under a certain value (near 25keV$\cdot nm^{-1}$). Meanwhile, there are more point defects produced by SHI than the amount of recovery when Se is larger than this value. Additionally, the evolution of different kinds of defects is investigated. The results indicate that the evolution of V_C and I_C is similar to the evolution of total point defects under different Se. Moreover, when Se is lower than this value (near 25keV$\cdot nm^{-1}$), the decrease of V_{Si} and I_{Si} is almost equal to the increment of C_{Si} and Si$_C$, respectively. Consequently, the defect recovery induced by SHI is mainly connected with the homogeneous recombination of the carbon defects, while the probabilities of heterogeneous recombination is mainly dependent on the silicon defects.

Declaration of competing interest

The authors declare that they have no known competing financial interests or personal relationships that could have appeared to influence the work reported in this paper.

Acknowledgments

This work was supported by Science Challenge Project No. TZ2018004, the National Natural Science Foundation of China (Grant No. 11835006, 11775167, 11690040, 11690043, 11975179, 11705137), and China Postdoctoral Science Foundation (No. 2019M663738).

References

[1] S.J. Zinkle, L.L. Snead, Influence of irradiation spectrum and implanted ions on the amorphization of ceramics, Nucl. Instrum. Methods Phys. Res. Sect. B Beam Interact. Mater. Atoms 116 (1–4) (1996) 92–101, https://doi.org/10.1016/0168-583X(96)00016-X.
[2] C.H. Park, B.H. Cheong, K.H. Lee, K.J. Chang, Structural and electronic properties of cubic, 2H, 4H, and 6H SiC, Phys. Rev. B 49 (7) (1994) 4485, https://doi.org/10.1103/PhysRevB.49.4485.
[3] P. Fenici, A.J. Frias Rebelo, R.H. Jones, A. Kohyama, L.L. Snead, Current status of SiC/SiC composites R & D, J. Nucl. Mater. 258 (1998) 215–225, https://doi.org/10.1016/S0022-3115(98)00303-1.
[4] R.A. Verrall, M.D. Vlajic, V.D. Krstic, Silicon carbide as an inert-matrix for a thermal reactor fuel, J. Nucl. Mater. 274 (1–2) (1999) 54–60, https://doi.org/10.1016/S0022-3115(99)00089-6.
[5] W. Jiang, W.J. Weber, S. Thevuthasan, D.E. McCready, Damage accumulation and annealing in 6H-SiC irradiated with Si+, Nucl. Instrum. Methods Phys. Res. Sect. B Beam Interact. Mater. Atoms 143 (3) (1998) 333–341, https://doi.org/10.1016/S0168-583X(98)00381-4.
[6] M. Backman, M. Toulemonde, O.H. Pakarinen, N. Juslin, F. Djurabekova, K. Nordlund, Molecular dynamics simulations of swift heavy ion induced defect recovery in SiC, Comput. Mater. Sci. 67 (2013) 261–265, https://doi.org/10.1016/j.commatsci.2012.09.010.
[7] E. Zarkadoula, G. Samolyuk, W.J. Weber, Effects of electron-phonon coupling

and electronic thermal conductivity in high energy molecular dynamics simulations of irradiation cascades in nickel, Comput. Mater. Sci. 162 (2019) 156–161, https://doi.org/10.1016/j.commatsci.2019.02.039.
[8] R. Devanathan, W.J. Weber, T. Diaz De La Rubia, Computer simulation of a 10 keV Si displacement cascade in SiC, Nucl. Instrum. Methods Phys. Res. Sect. B Beam Interact. Mater. Atoms 141 (1–4) (1998) 118–122, https://doi.org/10.1016/S0168-583X(98)00084-6.
[9] L. Malerba, J.M. Perlado, Molecular dynamics simulation of irradiation-induced amorphization of cubic silicon carbide, J. Nucl. Mater. 289 (1–2) (2001) 57–70, https://doi.org/10.1016/S0022-3115(00)00684-X.
[10] F. Gao, W.J. Weber, Recovery of close Frenkel pairs produced by low energy recoils in SiC, J. Appl. Phys. 94 (7) (2003) 4348–4356, https://doi.org/10.1063/1.1605254.
[11] D.E. Farrell, N. Bernstein, W.K. Liu, Thermal effects in 10 keV Si PKA cascades in 3C-SiC, J. Nucl. Mater. 385 (3) (2009) 572–581, https://doi.org/10.1016/j.jnucmat.2009.01.036.
[12] W. Li, L. Wang, L. Bian, F. Dong, M. Song, J. Shao, S. Jiang, H. Guo, Threshold displacement energies and displacement cascades in 4H-SiC: molecular dynamic simulations, AIP Adv. 9 (5) (2019), https://doi.org/10.1063/1.5093576, 055007.
[13] H. Xue, Y. Zhang, W.J. Weber, In-cascade ionization effects on defect production in 3C silicon carbide, Mater. Res. Lett. 5 (7) (2017) 494–500, https://doi.org/10.1080/21663831.2017.1334241.
[14] A. Audren, I. Monnet, D. Gosset, Y. Leconte, X. Portier, L. Thomé, F. Garrido, A. Benyagoub, M. Levalois, N. Herlin-Boime, C. Reynaud, Effects of electronic and nuclear interactions in SiC, Nucl. Instrum. Methods Phys. Res. Sect. B Beam Interact. Mater. Atoms 267 (6) (2009) 976–979, https://doi.org/10.1016/j.nimb.2009.02.033.
[15] A. Benyagoub, A. Audren, L. Thomé, F. Garrido, Athermal crystallization induced by electronic excitations in ion-irradiated silicon carbide, Appl. Phys. Lett. 89 (24) (2006) 241914, https://doi.org/10.1063/1.2405410.
[16] V.A. Skuratov, J.O. Connell, A.S. Sohatsky, J. Neethling, TEM study of damage recovery in SiC by swift Xe ion irradiation, Nucl. Instrum. Methods Phys. Res. Sect. B Beam Interact. Mater. Atoms 327 (2014) 89–92, https://doi.org/10.1016/j.nimb.2013.10.082.
[17] A. Benyagoub, Quantitative analysis of the epitaxial recrystallization effect induced by swift heavy ions in silicon carbide, Nucl. Instrum. Methods Phys. Res. Sect. B Beam Interact. Mater. Atoms 365 (2015) 376–379, https://doi.org/10.1016/j.nimb.2015.07.027.
[18] A. Debelle, L. Thomé, I. Monnet, F. Garrido, O.H. Pakarinen, W.J. Weber, Ionization-induced thermally activated defect-annealing process in SiC, Phys. Rev. Mater. 3 (6) (2019), https://doi.org/10.1103/PhysRevMaterials.3.063609, 063609.
[19] X. Wang, J. Li, J. Wang, J. Song, F. Zhao, H. Tang, B. Li, A. Xiong, Microstructure investigation of damage recovery in SiC by swift heavy ion irradiation, Mater. Des. Process. Commun. 1 (5) (2019) e87, https://doi.org/10.1002/mdp2.87.
[20] Y. Zhang, H. Xue, E. Zarkadoula, R. Sachan, C. Ostrouchov, P. Liu, X. lin Wang, S. Zhang, T.S. Wang, W.J. Weber, Coupled electronic and atomic effects on defect evolution in silicon carbide under ion irradiation, Curr. Opin. Solid State Mater. Sci. 21 (6) (2017) 285–298, https://doi.org/10.1016/j.cossms.2017.09.003.
[21] Y. Zhang, R. Sachan, O.H. Pakarinen, M.F. Chisholm, P. Liu, H. Xue, W.J. Weber, Ionization-induced annealing of pre-existing defects in silicon carbide, Nat. Commun. 6 (1) (2015) 8049, https://doi.org/10.1038/ncomms9049.
[22] L. Thomé, A. Debelle, F. Garrido, P. Trocellier, Y. Serruys, G. Velisa, S. Miro, Combined effects of nuclear and electronic energy losses in solids irradiated with a dual-ion beam, Appl. Phys. Lett. 102 (14) (2013) 141906, https://doi.org/10.1063/1.4801518.
[23] L. Thomé, G. Velişa, A. Debelle, S. Miro, F. Garrido, P. Trocellier, Y. Serruys, Behavior of nuclear materials irradiated with a dual ion beam, Nucl. Instrum. Methods Phys. Res. Sect. B Beam Interact. Mater. Atoms 326 (2014) 219–222, https://doi.org/10.1016/j.nimb.2013.09.054.
[24] W.J. Weber, D.M. Duffy, L. Thomé, Y. Zhang, The role of electronic energy loss in ion beam modification of materials, Curr. Opin. Solid State Mater. Sci. 19 (1) (2015) 1–11, https://doi.org/10.1016/j.cossms.2014.09.003.
[25] A. Benyagoub, A. Audren, Study of the damage produced in silicon carbide by high energy heavy ions, Nucl. Instrum. Methods Phys. Res. Sect. B Beam Interact. Mater. Atoms 267 (8–9) (2009) 1255–1258, https://doi.org/10.1016/j.nimb.2009.01.026.
[26] S. Sorieul, X. Kerbiriou, J.M. Costantini, L. Gosmain, G. Calas, C. Trautmann, Optical spectroscopy study of damage induced in 4H-SiC by swift heavy ion irradiation, J. Phys. Condens. Matter 24 (12) (2012) 125801, https://doi.org/10.1088/0953-8984/24/12/125801.
[27] I.T. Todorov, W. Smith, K. Trachenko, M.T. Dove, DL_POLY_3: new dimensions in molecular dynamics simulations via massive parallelism, J. Mater. Chem. 16 (20) (2006) 1911–1918, https://doi.org/10.1039/B517931A.
[28] A.E. Ismail, J.A. Greathouse, P.S. Crozier, S.M. Foiles, Electron-ion coupling effects on simulations of radiation damage in pyrochlore waste forms, J. Phys. Condens. Matter 22 (22) (2010) 225405, https://doi.org/10.1088/0953-8984/22/22/225405.
[29] D.M. Duffy, A.M. Rutherford, Including the effects of electronic stopping and electron-ion interactions in radiation damage simulations, J. Phys. Condens. Matter 19 (1) (2006), 016207, https://doi.org/10.1088/0953-8984/19/1/016207.
[30] H. Hensel, H.M. Urbassek, Preferential effects in low-energy Si bombardment of SiC, Nucl. Instrum. Methods Phys. Res. Sect. B Beam Interact. Mater. Atoms 142 (3) (1998) 287–294, https://doi.org/10.1016/S0168-583X(98)00284-5.
[31] I.T. Todorov, W. Smith, U.K. Cheshire, The DL POLY 4 User Manual, STFC, STFC Daresbury Lab, Daresbury, Warrington, Cheshire, WA4 4AD, United Kingdom, 2011. Version. 4(0).
[32] A.M. Rutherford, D.M. Duffy, The effect of electron-ion interactions on radiation damage simulations, J. Phys. Condens. Matter 19 (49) (2007) 496201, https://doi.org/10.1088/0953-8984/19/49/496201.
[33] C.P. Race, D.R. Mason, M.W. Finnis, W.M.C. Foulkes, A.P. Horsfield, A.P. Sutton, The treatment of electronic excitations in atomistic models of radiation damage in metals, Rep. Prog. Phys. 73 (11) (2010) 116501, https://doi.org/10.1088/0034-4885/73/11/116501.
[34] M. Toulemonde, C. Dufour, A. Meftah, E. Paumier, Transient thermal processes in heavy ion irradiation of crystalline inorganic insulators, Nucl. Instrum. Methods Phys. Res. Sect. B Beam Interact. Mater. Atoms 166 (2000) 903–912, https://doi.org/10.1016/S0168-583X(99)00799-5.
[35] M. Toulemonde, W. Assmann, C. Dufour, A. Meftah, F. Studer, C. Trautmann, Experimental phenomena and thermal spike model description of ion tracks in amorphisable inorganic insulators, Mat. Fys. Medd. 52 (2006) 263–292.
[36] A. Mozumder, Track-core radius of charged particles at relativistic speed in condensed media, J. Chem. Phys. 60 (3) (1974) 1145–1148, https://doi.org/10.1063/1.1681125.
[37] M. Toulemonde, J.M. Costantini, C. Dufour, A. Meftah, E. Paumier, F. Studer, Track creation in SiO2 and BaFe12O19 by swift heavy ions: a thermal spike description, Nucl. Instrum. Methods Phys. Res. Sect. B Beam Interact. Mater. Atoms 116 (1–4) (1996) 37–42, https://doi.org/10.1016/0168-583X(96)00007-9.
[38] B. Gervais, S. Bouffard, Simulation of the primary stage of the interaction of swift heavy ions with condensed matter, Nucl. Instrum. Methods Phys. Res. Sect. B Beam Interact. Mater. Atoms 88 (4) (1994) 355–364, https://doi.org/10.1016/0168-583X(94)95384-8.
[39] W. Liao, C. He, H. He, Molecular dynamics simulation of displacement damage in 6H-SiC, Radiat. Eff. Defect Solid 174 (9–10) (2019) 729–740, https://doi.org/10.1080/10420150.2019.1649260.
[40] S. Zhao, G. Ran, Y. Guo, Q. Han, S. Liu, F. Gao, Study on the mechanism of helium platelets formation at low temperatures in SiC from the perspective of atomic diffusion, J. Nucl. Mater. 542 (2020) 152507, https://doi.org/10.1016/j.jnucmat.2020.152507.
[41] M.J. Zheng, N. Swaminathan, D. Morgan, I. Szlufarska, Energy barriers for point-defect reactions in 3C-SiC, Phys. Rev. B 88 (5) (2013), 054105, https://doi.org/10.1103/PhysRevB.88.054105.
[42] G. Roma, J.P. Crocombette, Evidence for a kinetic bias towards antisite formation in SiC nano-decomposition, J. Nucl. Mater. 403 (1–3) (2010) 32–41, https://doi.org/10.1016/j.jnucmat.2010.06.001.
[43] T. Lingner, S. Greulich Weber, J.M. Spaeth, U. Gerstmann, E. Rauls, Z. Hajnal, T. Frauenheim, H. Overhof, Structure of the silicon vacancy in 6H-SiC after annealing identified as the carbon vacancy–carbon antisite pair, Phys. Rev. B 64 (24) (2001) 245212, https://doi.org/10.1103/PhysRevB.64.245212.
[44] F.X. Zhang, Y. Tong, H. Xue, J.K. Keum, Y. Zhang, A. Boulle, A. Debelle, W.J. Weber, Strain engineering 4H-SiC with ion beams, Appl. Phys. Lett. 114 (22) (2019) 221904, https://doi.org/10.1063/1.5109226.